MOTION-CORRECTION TECHNIQUES FOR STANDING EQUINE MRI

ALEXIA L. MCKNIGHT, DVM, ARMANDO MANDUCA, PHD, JOEL P. FELMLEE, PHD, PHILIP J. ROSSMAN, MS, KIARAN P. MCGEE, PHD, RICHARD L. EHMAN, MD

Magnetic resonance imaging (MRI) of the distal extremities of the standing, sedated horse would be desirable if diagnostic quality images could be obtained. With the availability of extremity and special purpose magnet designs on the market, a system to safely accommodate the standing horse may gain increasing popularity. This paper considers the issue of motion that will need to be addressed to achieve successful, diagnostic quality images. The motion of the carpus and tarsus of five standing, sedated horses was quantified. The obtained motion records were then used to induce motion in cadaveric joint specimens during several MRI scans. The measured dorsal–palmar/plantar, medial–lateral, and proximal–distal random wobbling motions in the standing sedated horse were several centimeters in magnitude and generated severe motion-artifacts during axial MRI of the cadaveric specimens. Two retrospective motion-correction techniques (autocorrection and navigator-based adaptive correction) were used to correct the corrupted images. The motion artifacts were nearly eliminated with the use of both techniques in series. Although significant hurdles remain, these results suggest promise for allowing diagnostic quality MRI of the carpus and tarsus in the standing horse. *Veterinary Radiology & Ultrasound, Vol. 45, No. 6, 2004, pp 513–519.*

Key words: equine, magnetic resonance imaging, motion, motion correction.

Introduction

MAGNETIC RESONANCE IMAGING (MRI) in veterinary medicine has often been limited to small animals under general anesthesia.[1] Recent constraints include magnet designs that cannot easily accommodate large animals and the inability to obtain high-quality images in nonanesthetized animals because of motion. As these constraints are overcome, the diagnostic benefits of MRI may expand to large and small animals imaged only under sedation. High-quality conventional MR examinations of the distal limbs of the standing horse are within the realm of possibilities.

Magnets designed to accommodate the lower limb of a standing horse are nearing market availability. Because of inherent size limitations of the horse, it is likely that the field strength of the system will be in the low- to mid-field range. Even with conventional high-field strength MR scanners (where signal-to-noise ratio (SNR) is higher) physiologic and nonphysiologic motion can cause significant image quality degradation. Longer scan times help regain SNRs in lower field strength systems—but at the price of increased susceptibility to motion artifacts. Therefore, motion is a critical problem to address for acceptable image quality in a standing, sedated horse.

Considerable research to reduce motion artifacts caused by translational and rotational motion of the body during MRI is ongoing.[2–20] Motion artifacts are particularly problematic for cardiac imaging,[21] diffusion weighted imaging,[22–24] functional imaging,[7,25] upper abdominal imaging,[21,26] musculoskeletal imaging,[15] and examinations on pediatric,[3] neurologic,[27] and elderly patients.

There are several methods for motion correction in MRI. Each has advantages and disadvantages, and its usefulness is related to the type of motion and the application. Techniques during acquisition include fast scanning sequences, various reordering,[28] resampling,[29] and gating[21] of the *k*-space data, gradient moment nulling,[30] and presaturation.[31] Some extremely fast scanning sequences, such as echo planar imaging, for example, work well for brain and upper abdominal studies, but are associated with higher susceptibility artifacts so that heterogeneous musculoskeletal tissues are difficult to image with these pulse sequences. Furthermore, not all scanners have the hardware or software capabilities for some fast sequences. Periodicity of motion, as in the respiratory and cardiac cycles, dictate the use of specialized gated data acquisition sequences for motion compensation, but these are not applicable in standing equine MRI. There are many retro-

From the University of Pennsylvania School of Veterinary Medicine, New Bolton Center, Kennett Square, PA 19348 (McKnight) and Department of Physiology and Biophysics (Manduca) and Department of Radiology, Mayo Clinic, Rochester, MN 55905 (Felmlee, Rossman, McGee, Ehman).

Oral presentation given at the ACVR Annual Conference, Honolulu, HI 2001 on the Feasibility of Standing Equine MRI.

Address correspondence and reprint requests to Alexia L. McKnight, DVM, School of Veterinary Medicine, University of Pennsylvania, New Bolton Center, 382 West Street Rd., Kennett Square, PA 19348.
E-mail: alexiajl@vet.upenn.edu

Received November 14, 2003; accepted for publication April 26, 2004.
doi: 10.1111/j.1740-8261.2004.04087.x

spective techniques[4,8,10,32–35] that can aid in the correction of motion-corrupted data that may be well suited for equine applications.

This paper evaluates the use of two different retrospective motion-correction techniques as they pertain to the standing, sedated horse using conventional spin echo pulse sequences: navigator echoes[4,7,8,36] and autocorrection.[10,35] Navigator echoes are incorporated into the imaging pulse sequence and track motion during an exam, which is then used to correct the data retrospectively (see Fig. 1A). Navigator echoes are effective for in-plane, nondeforming global motions as in musculoskeletal imaging,[15] but they require the use of a special pulse sequence for data acquisition. The autocorrection technique corrects image data retrospectively without a priori motion history. The motion-corrupted image itself provides the information necessary for correction. An image metric and an iterative algorithm are used to quantify and minimize motion artifacts given a motion-corrupted image (see Fig. 1B). Autocorrection has been proven useful for imaging the shoulder where respiratory motion because of respiration or motion from relaxation can seriously degrade image quality.[10]

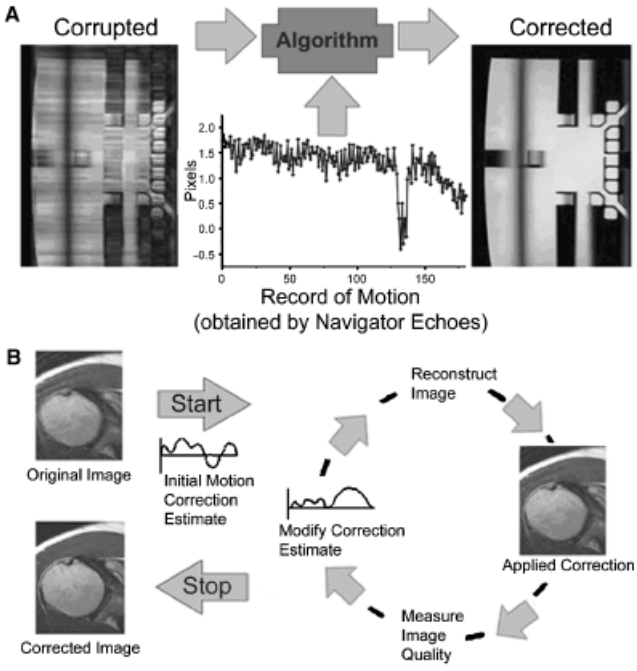

FIG. 1. (A) This schematic illustrates navigator echo correction. A special pulse sequence acquires a navigator echo at each view of the scan used to map the position of the object or body in one or more degrees of freedom during every phase encoding view. The middle graph represents the results of navigator echoes acquired during the scan of a phantom. The pixel displacements in a specific direction are shown along the *y*-axis, and the numbers of views are shown along the *x*-axis. The motion-corrupted image of the phantom is corrected using this information. The maximum pixel displacements in this example are less than 2.5 pixels. The displacements in the standing horse are as large as 30–40 pixels. (B) This schematic illustrates the process of autocorrection. In this technique, the motion occurring during a scan is not measured. The raw motion corrupted *k*-space data is analyzed, and the motion is deduced using an image quality metric that quantifies motion artifacts. The algorithm estimates trial corrections and evaluates their result on image quality. This process is iterated many times until the image metric is optimized.

As the foot of a standing horse remains on a nonmoving surface, it is considered to least likely cause significant motion artifacts and be the easiest region to successfully image. Therefore, the carpus and tarsus were chosen for examination. These joints are more susceptible to motion artifacts and are near the proximal limit of the limb that can still be imaged while the horse is standing. The objectives for this paper are to (1) observe and quantify motion in the carpus and tarsus while simulating a standing equine MR examination, (2) apply these measured "standing" motions to cadaver limbs during MRI, and (3) assess the ability of navigator echoes and autocorrection to correct the obtained motion-corrupted images.

Methods

To quantify the motion of the carpus and tarsus that would occur during an MRI examination of the standing horse, we first built a full-sized wooden model of a magnet designed for this purpose to simulate a standing exam. The model represents a small, 0.3 T open bore permanent magnet.* Four highly reflective spherical markers were placed on the carpus and tarsus of five thoroughbred horses that were then centered within the bore of the model magnet. A total of 10 motion records (five carpus and five tarsus records) were obtained by optically tracking each marker. Standing sedation was achieved in all five horses with a combination of acepromazine (20–25 mg) and detomidine (2–4 mg).

The model magnet had windows in two of its three sides so that three–dimensional (3D) motions of the carpus and tarsus could be monitored. This was done by using Digital Motion Analysis Software (DMAS®),† an optical high-resolution 3D motion acquisition technique by Spica Technologies, Inc. This system used two progressive scan digital video cameras‡ placed approximately 90° apart that were focused on the same four markers. The cameras were set to obtain images at a frequency of 20 Hz for a total of 10 min on each joint. The DMAS® software has been independently tested at the University of Utah and shown to have a mean error of 0.004% of the field of view. This setup included a 25-cm field of view, allowing us to detect motion as small as 14 μm. This information was subsequently analyzed by DMAS® to obtain motion records.

These motion records were used to simulate the actual standing motion in cadaver specimens of the carpus and tarsus during MRI. This was accomplished by building a 2D computer-controlled MRI motion simulator that precisely displaced the cadaveric specimens in the medial to

*Magna-Lab Inc., Syosset, NY.
†Kihei, Maui, HI.
‡Pulnix America, Sunnyvale, CA.

lateral and the dorsal to palmar/plantar motions according to the motion record files. The motion simulator displaced the specimens at 20 Hz, corresponding to the frequency of the acquired data. Time permitted for five of the 10 different obtained motion records to be used as input into the motion simulator. The five records that were chosen did not exceed the motion simulator's acceleration limits (corresponding to a peak velocity of approximately 7 cm/s).

MRI of the mechanically moving specimens was performed in a conventional 1.5 T GE Signa§ superconducting system using a head coil. Spin echo pulse sequences, containing two orthogonal navigator echoes, were applied. The navigator echoes preceded each imaging TR and were used to measure x and y displacement throughout the scan period so that adaptive motion correction could be made. The image matrix was 256×256; T1-, T2-, and proton density-weighted images were acquired, and the field of view was 20–21 cm. Scan times were either 3 min 26 s (for the T1-weighted scans) or 8 min 56 s (for the proton- and T2-weighted scans). Static images of each sample were also obtained with the same acquisition parameters.

For the autocorrection technique, image entropy was measured as the image quality parameter.[10,35] The methodology used was similar to that described by Manduca et al.,[10] with the exception that translations in x and y were searched for simultaneously using a simplex algorithm.[37] Individual autocorrection run times were approximately 65 min. For this study on a Sun Enterprise 450‖ with four 400 MHz processors and 4 GB RAM. Two iterations of the autocorrection scheme were performed on each case to improve performance.

All five motion corrupted MR images were processed using navigator echoes and the autocorrection technique. Both techniques were also tried in combination to further evaluate for optimal correction. Four radiologists were then asked to review each of the 20 images and assign an observer score according to the following scale: 0 = no motion artifacts detected; 1 = minimal artifacts, image considered diagnostic quality; 2 = mild-to-moderate artifacts, image considered nondiagnostic; 3 = severe artifacts, completely nondiagnostic.

Results

Four examples of the obtained motion records from the carpus and tarsus are shown in Fig. 2. Random oscillatory motions are present in the medial–lateral and dorsal–palmar/plantar directions throughout the 10-min period. As expected, much smaller motions are in the proximal–distal direction. One interesting finding in all horses (in addition to the random motions described above) is very regular, sinusoidal oscillations at a rate of approximately 10/min (see inset, Fig. 2B). The displacements of these oscillations averaged 2–5 mm and result from the respiratory cycle.

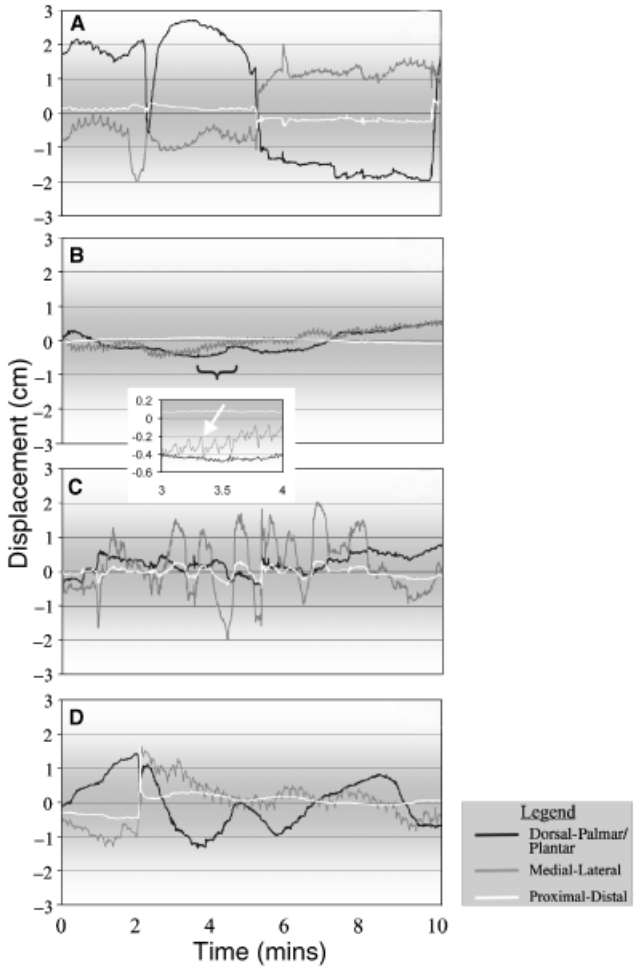

FIG. 2. Ten-minute motion record results obtained from standing sedated horses. (A)The motion occurring in the carpus of Horse 5, considered "typical." (B) The motion record from the carpus of Horse 4, containing the least amount of motion of all experiments. The inset shows an enlarged 1-min section. The white arrow is pointing to one of the typical oscillatory peaks that represent medial to lateral motion from the respiratory cycle that was relatively distinct in most of the horses. (C)The motion record from the tarsus of Horse 3, also considered "typical." (D) A motion record from the tarsus of Horse 5. Note the abrupt rise in the proximal–distal motion as the horse shifted his weight, as well as the distinct oscillatory pattern in the medial–lateral direction from the respiratory cycle.

The maximum and average peak-to-peak displacements during the 10-min period for the carpus and tarsus are illustrated in Fig. 3. The majority of all the maximum peak-to-peak displacements in the medial–lateral and dorsal–palmar/plantar directions were less than 4 cm; however, in several instances the displacements exceeded 4 cm and in one was 7.8 cm. The majority of peak-to-peak displacements in the proximal–distal direction were less than 1 cm, with two instances of maximum displacements reaching 2 and 3 cm. The differences existing between horses is illustrated in Fig. 2A–D. The average displacement was

§General Electric, Milwaukee, WI.
‖Sun System, Santa Clara, CA.

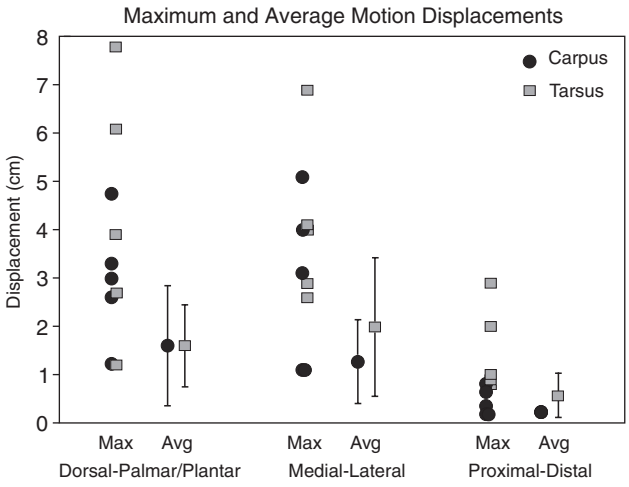

FIG. 3. The maximum and average peak to peak displacements of the carpus and tarsus in the medial–lateral, dorsal–palmar/plantar and proximal–distal directions for each of the 10 motion records is shown here. The large majority of the maximum and average dorsal-proximal/plantar and medial–lateral motions were less than 4 cm, with several instances reaching between 5 and 8 cm. The large majority of the maximum and average proximal–distal displacements were less than 1 cm, with two instances reaching 2 and 3 cm. The average displacement is reported as the average of all ten 95% confidence intervals of the mean for each motion record.

calculated by using the 95% confidence interval about the mean for each motion record. The average of all ten 95% confidence intervals in the dorsal–palmar/plantar direction was 1.6 ± 1.2 cm for the carpus, and 1.6 ± 0.8 cm for the tarsus. In the medial–lateral direction, the average of all ten 95% confidence intervals was 1.26 cm with a standard deviation of ± 0.9 for the carpus, and an average of 2.0 cm ± 1.4 for the tarsus. The average of all ten 95% confidence intervals in the proximal–distal direction was 0.2 cm with a standard deviation of ± 0.1 cm for the carpus and 0.6 ± 0.5 cm for the tarsus.

Transverse images of the carpus and tarsus of four of the five scans are shown in Fig. 4A–D. The images on the left correspond to the scans obtained while applying the medial–lateral and dorsal–palmar/plantar motion records seen in Fig. 2A–D. Note that the scan times were less than the full 10-min motion records; Fig. 4A–C were from the first 8 min 56 s, and Fig. 4D was from the first 3 min 26 s of the motion records. The images obtained after correction from a combination of both navigator echo correction and autocorrection are shown in the middle column of Fig. 4A–D. The images on the right are the static (no motion) images for comparison. The corrected images are comparable in quality to the static images, and only minimal motion artifacts remain in some cases.

Figure 5 presents the average observer scores for each of the images. All five of the scans with the applied motions from the records obtained from the standing horses are considered completely nondiagnostic with moderate-to-severe motion artifacts. Autocorrection alone improved

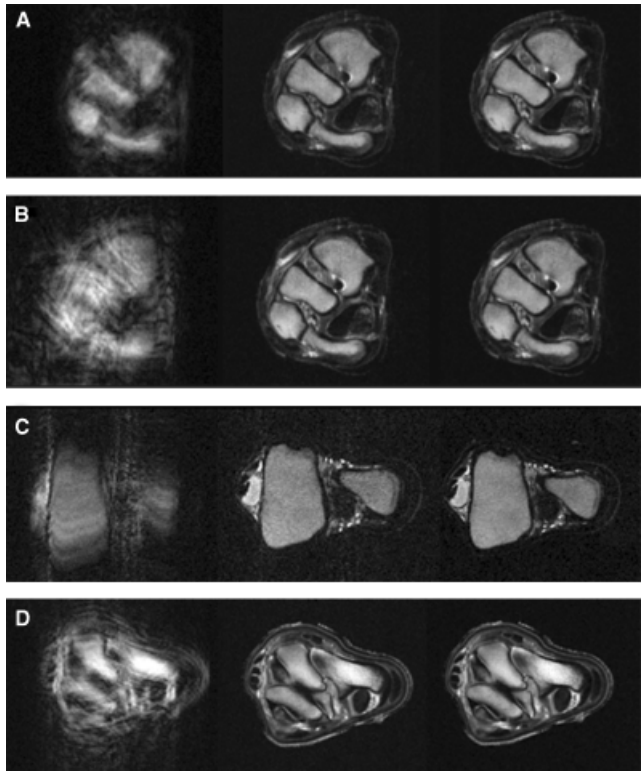

FIG. 4. The images on the left are from the magnetic resonance exams obtained while moving the carpus (A, B) and tarsus (C, D) according to their corresponding motion records shown in Fig. 2. The scans in (A, B) are proton density weighted, (C) is T2-weighted, and (D) is T1-weighted. The images in the middle result from the combination of adaptive motion correction using both navigator echoes and autocorrection. The static, no motion images are on the right for comparison.

image quality, but not to a diagnostic level. Navigator echo correction alone was considered to improve image quality to a diagnostic quality in four of the five cases. The combination of the two algorithms further improved image quality to where most observers rated four of the five cases as having no motion artifacts present.

Figure 6 shows an example of the difference in image improvement by navigator echo correction alone (6B), autocorrection alone (6C), and the combined navigator echo/autocorrection technique (6D). Both individual corrections have improved image quality, but motion artifacts have been further reduced by combining the two algorithms. The superficial medial and lateral vessels, for example, are well demarcated only following the combined corrections.

Discussion

Any motion that is greater than approximately half the pixel resolution of the MR image can degrade image quality. As an example, an image with a 20 cm field of view and a 256×256 image matrix would have an in-plane resolution of 0.78 mm. This would mean that motions as small as 0.4 mm could potentially create visible artifacts. The

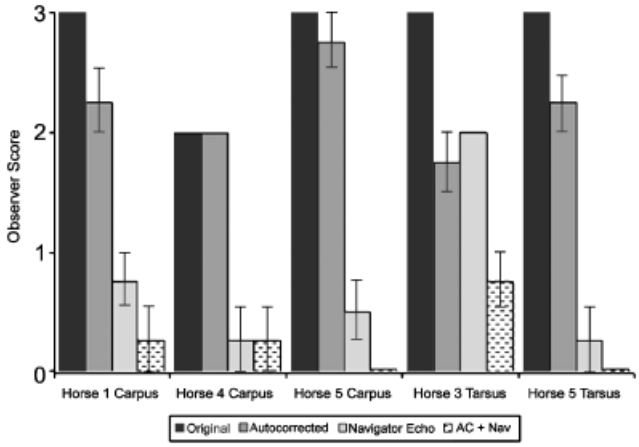

FIG. 5. The average of the observer scores from the four radiologists are shown for the original motion corrupted image, and each of the navigator corrected, autocorrected, and combined navigator and autocorrected images. Observer score: 0 = no motion artifacts detected; 1 = minimal artifacts, image considered diagnostic quality; 2 = mild-to-moderate artifacts, image considered nondiagnostic; 3 = severe artifacts, completely nondiagnostic. All five original scans were considered nondiagnostic, four of them with severe motion artifacts present. The autocorrected images only generally improved the image quality somewhat, but not to a diagnostic quality. Four of the five navigator echo corrected images markedly improved to a diagnostic quality. Most observers rated four of the five combined autocorrected and navigator echo corrected images as having no motion artifacts detected. Error bars represent standard error of the mean. Values without error bars indicate all four reviewers reported the same score.

random, wobbling motions that were measured in the carpus and tarsus of 10 standing, sedated horses were up to 40–50 mm.

The degree of motion artifacts present in the image is also heavily dependent upon the timing of the motion relative to the filling of *k*-space. One millimeter displacements occurring during the acquisition of the center of *k*-space will have a much more deleterious effect than during acquisition of the edges of *k*-space. The measurements presented here, however, show that the wobbling motion occurring in the standing, sedated horse are continuous, random, and of such large magnitude that they will likely always be problematic. The motions occurring secondary to the respiratory cycle alone were shown to be 2–5 mm displacements and are enough to corrupt the image and render it nondiagnostic.

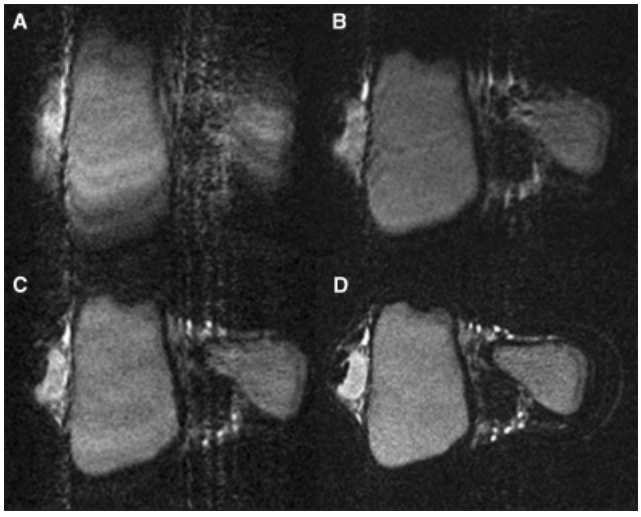

FIG. 6. Original motion corrupted T2-weighted image from the tarsus of Horse 3 (A), and correction results by navigator echoes alone (B), autocorrection alone (C), and the navigator echoes in combination with autocorrection (D).

Given that the motions in the carpus and tarsus are very large relative to the in-plane image resolution, successful MRI of these regions will be dependent on some type of motion correction. Although motion correction is a popular topic of MR research, we are unaware of other publications reporting correction of displacements as large as reported in this study. We note that the combination of navigator echoes and autocorrection is surprisingly powerful and capable of converting severely motion corrupted, completely nondiagnostic image data into diagnostic images.

The correlation between the motion records that were used to move the cadaver specimens and the resultant navigator record was not measured. However, the movement was asynchronous because the time resolution of the motion records was much finer than the navigator pulses in each imaging TR. This was performed in order to include any intraview effects on motion correction. The results of the study suggest that intraview motion in the standing horse will not be problematic.

The computational time for correction in this study was nearly instantaneous with the navigator technique. The 65 min autocorrection computations were excessively long in this study. This time can be significantly shortened with highly optimized FFTs, faster processors, and other techniques[38] that were not used.

There are several limitations and other assumptions of this study that impact the clinical usefulness of this work. First, the through-plane motions were ignored. Although the proximal–distal motions were much smaller in magnitude (often less than 1.5 cm) than the medial–lateral and dorsal–palmar/plantar motions, they were significantly large relative to the 3 mm through-plane resolution (or slice thickness). Through-plane motions are more challenging to correct and are critical in order to image the sagittal and dorsal planes where all medial–lateral and dorsal–palmar/plantar motions, respectively, are through plane. Next, the motions were assumed to be rigid-body motions. Any small deformations of the joint may affect image quality. Finally, all motions were assumed to be translational motions, and a small degree of rotational motion may be present that would further complicate the correction process.

It is also important to consider that we used a conventional 1.5 T superconducting magnet in this study. This scanner will likely have a larger homogeneous field and a

higher SNR than a system designed for the standing horse. The size of the homogeneous field is important because motions that extend beyond the homogeneous field of the magnet (and beyond the imaging field of view) are more difficult to correct. Furthermore, the SNR in a 1.5 T system will also likely be greater than that available in a magnet designed for the standing horse. The increased noise would negatively affect both navigator echo and autocorrection techniques, but it is not known to what extent.

Although increasing the scan time can increase the SNR for improved image quality, it also makes the scan more susceptible to motion artifacts. For this reason, we chose to use proton density-, T2-, and T1-weighted scans with times (8 min 56 s, 8 min 56 s, and 3 min 26 s, respectively) longer than necessary so that they would better reflect the longer scan times typical of a lower field strength system. The results indicate that corrections of realistic standing equine motions are possible with these long scan times.

Conclusion

The motion records obtained from the carpus and the tarsus of five standing, sedated horses indicate large medial–lateral, dorsal–palmar/plantar, and proximal–distal random wobbling motions. Smaller regular, cyclic medial–lateral motions secondary to the respiratory cycle also exist. When applied to cadaveric specimens, these motions rendered the MR images completely nondiagnostic with varying degrees of motion artifacts. For in-plane motions, autocorrection and navigator-based adaptive correction techniques together resulted in diagnostic image quality even in the presence of severe motion. In our study, navigator echoes appeared to provide better "coarse tuning" of the images. Autocorrection appeared to provide the necessary "fine tuning." Further work is needed to determine the best correction technique for through-plane motions before conventional, diagnostic quality musculoskeletal imaging of the distal limbs of the standing horse could be performed.

Significant hurdles remain, including a well-designed magnet, that still need to be addressed before clinical imaging is expected to be acceptable. However, these results suggest promise for diagnostic quality MRI of the carpus and tarsus in the standing, sedated horse using conventional spin echo pulses.

ACKNOWLEDGMENTS

The authors would like to acknowledge Mikael Brommels of Spica Technologies for his invaluable assistance with the DMAS motion tracking system. We would also like to gratefully acknowledge the faculty and staff of the Mayo MRI Research Lab, Mayo Bioengineering Department, and New Bolton Center, who helped with this project. Part of this work was funded by NIH Grant #EB000229.

REFERENCES

1. McKnight LA.Veterinary MRI Statistics, in American College of Veterinary Radiology Annual Conference, Banff, Alberta, Canada.
2. Peshkovsky A, Knuth KH, Helpern JA. Motion correction in MRI using an apparatus for dynamic angular position tracking (ADAPT). Magn Reson Med 2003;49:138–143.
3. Forbes KP, Pipe JG, Karis JP, Farthing V, Heiserman JE. Brain imaging in the unsedated pediatric patient: comparison of periodically rotated overlapping parallel lines with enhanced reconstruction and single-shot fast spin-echo sequences. Am J Neuroradiol 2003;24:794–798.
4. Welch EB, Manduca A, Grimm RC, Ward HA, Jack CR, Jr. Spherical navigator echoes for full 3D rigid body motion measurement in MRI. Magn Reson Med 2002;47:32–41.
5. Norris DG, Driesel W. Online motion correction for diffusion-weighted imaging using navigator echoes: application to RARE imaging without sensitivity loss. Magn Reson Med 2001;45:729–733.
6. Mathiak K, Posse S. Evaluation of motion and realignment for functional magnetic resonance imaging in real time. Magn Reson Med 2001;45:167–171.
7. Ward HA, Riederer SJ, Grimm RC, Ehman RL, Felmlee JP, Jack CR Jr. Prospective multiaxial motion correction for fMRI. Magn Reson Med 2000;43:459–469.
8. Wang Y, Ehman RL. Retrospective adaptive motion correction for navigator-gated 3D coronary MR angiography. J Magn Reson Imaging 2000;11:208–214.
9. McGee KP, Manduca A, Felmlee JP, Riederer SJ, Ehman RL. Image metric-based correction (autocorrection) of motion effects: analysis of image metrics. J Magn Reson Imaging 2000;11:174–181.
10. Manduca A, McGee KP, Welch EB, Felmlee JP, Grimm RC, Ehman RL. Autocorrection in MR imaging: adaptive motion correction without navigator echoes. Radiology 2000;215:904–909.
11. Schaffter T, Rasche V, Carlsen IC. Motion compensated projection reconstruction. Magn Reson Med 1999;41:954–963.
12. Pipe JG. Motion correction with PROPELLER MRI: application to head motion and free-breathing cardiac imaging. Magn Reson Med 1999;42:963–969.
13. Krishnan S, Chenevert TL, Helvie MA, Londy FL. Linear motion correction in three dimensions applied to dynamic gadolinium enhanced breast imaging. Med Phys 1999;26:707–714.
14. Mori S, van Zijl PC. A motion correction scheme by twin-echo navigation for diffusion-weighted magnetic resonance imaging with multiple RF echo acquisition. Magn Reson Med 1998;40:511–516.
15. McGee KP, Grimm RC, Felmlee JP, Rydberg JR, Riederer SJ, Ehman RL. The shoulder: adaptive motion correction of MR images. Radiology 1997;205:541–545.
16. Zuo CS, Jiang A, Buff BL, Mahon TG, Wong TZ. Automatic motion correction for breast MR imaging. Radiology 1996;198:903–906.
17. Wang Y, Rossman PJ, Grimm RC, Riederer SJ, Ehman RL. Navigator-echo-based real-time respiratory gating and triggering for reduction of respiration effects in three-dimensional coronary MR angiography. Radiology 1996;198:55–60.
18. Trouard TP, Sabharwal Y, Altbach MI, Gmitro AF. Analysis and comparison of motion-correction techniques in diffusion-weighted imaging. J Magn Reson Imaging 1996;6:925–935.
19. Spritzer CE, Keogan MT, DeLong DM, Dahlke J, MacFall JR. Optimizing fast spin echo acquisitions for hepatic imaging in normal subjects. J Magn Reson Imaging 1996;6:128–135.
20. Polzin JA, Korosec FR, Wedding KL, et al. Effects of through-plane myocardial motion on phase-difference and complex-difference measurements of absolute coronary artery flow. J Magn Reson Imaging 1996;6:113–123.
21. Ehman RL, McNamara MT, Pallack M, Hricak H, Higgins CB. Magnetic resonance imaging with respiratory gating: techniques and advantages. Am J Roentgenol 1984;143:1175–1182.

22. Ordidge RJ, Helpern JA, Qing ZX, Knight RA, Nagesh V. Correction of motional artifacts in diffusion-weighted MR images using navigator echoes. Magn Reson Imaging 1994;12:455–460.

23. Anderson AW, Gore JC. Analysis and correction of motion artifacts in diffusion weighted imaging. Magn Reson Med 1994;32:379–387.

24. Bosak E, Harvey PR. Navigator motion correction of diffusion weighted 3D SSFP imaging. J Magn Magn Mater 2001;12:167–176.

25. Le TH, Hu X. Retrospective estimation and correction of physiological artifacts in fMRI by direct extraction of physiological activity from MR data. Magn Reson Med 1996;35:290–298.

26. Korin HW, Ehman RL, Riederer SJ, Felmlee JP, Grimm RC. Respiratory kinematics of the upper abdominal organs: a quantitative study. Magn Reson Med 1992;23:172–178.

27. Marks MP, de Crespigny A, Lentz D, Enzmann DR, Albers GW, Moseley ME. Acute and chronic stroke: navigated spin-echo diffusion-weighted MR imaging. [erratum appears in Radiology 1996 Jul;200(1):289] Radiology 1996;199:403–408.

28. Bailes DR, Gilderdale DJ, Bydder GM, Collins AG, Firmin DN. Respiratory ordered phase encoding (ROPE): a method for reducing respiratory motion artefacts in MR imaging. J Comput Assist Tomogr 1985;9:835–838.

29. Sachs TS, Meyer CH, Irarrazabal P, Hu BS, Nishimura DG, Macovski A. The diminishing variance algorithm for real-time reduction of motion artifacts in MRI. Magn Reson Med 1995;34:412–422.

30. Hinks RS, Constable RT. Gradient moment nulling in fast spin echo. Magn Reson Med 1994;32:698–706.

31. Felmlee JP, Ehman RL. Spatial presaturation: a method for suppressing flow artifacts and improving depiction of vascular anatomy in MR imaging. Radiology 1987;164:559–564.

32. Lee CC, Jack CR Jr., Grimm RC, et al. Real-time adaptive motion correction in functional MRI. Magn Reson Med 1996;36:436–444.

33. Felmlee JP, Ehman RL, Riederer SJ, Korin HW. Adaptive motion compensation in MR imaging without use of navigator echoes. Radiology 1991;179:139–142.

34. Lenz GW, Haacke EM, White RD. Retrospective cardiac gating: a review of technical aspects and future directions. Magn Reson Imaging 1989;7:445–455.

35. Atkinson D, Hill DL, Stoyle PN, Summers PE, Keevil SF. Automatic correction of motion artifacts in magnetic resonance images using an entropy focus criterion. IEEE Trans Med Imaging 1997;16:903–910.

36. Ehman RL, Felmlee JP. Adaptive technique for high-definition MR imaging of moving structures. Radiology 1989;173:255–263.

37. Press WH, Teukosky SA, Vetterling WT, Flannery BP. Numerical Recipes in C: the Art of Scientific Computing, 2nd ed. Cambridge: Cambridge University Press, 1992.

38. Manduca A, McGee KP, Welch EB, Felmlee JP, Ehman RL. Fast automatic correction of motion artifacts in shoulder MRI, in medical imaging 2001: image processing, SPIE 4322, 2001; 853–859.